Title
Subdiffraction-resolution live-cell imaging for visualizing thylakoid membranes

Journal
The Plant Journal, 96(1)

ISSN
0960-7412

Authors
Iwai, Masakazu
Roth, Melissa S
Niyogi, Krishna K

Publication Date
2018-10-01

DOI
10.1111/tpj.14021

Peer reviewed

the plant journal

SEB Society for Experimental Biology

The Plant Journal (2018) doi: 10.1111/tpj.14021

TECHNICAL ADVANCE

Subdiffraction-resolution live-cell imaging for visualizing thylakoid membranes

Masakazu Iwai[1,2,*], Melissa S. Roth[2] and Krishna K. Niyogi[1,2,*]

[1]*Molecular Biophysics and Integrated Bioimaging Division, Lawrence Berkeley National Laboratory, Berkeley, CA 94720, USA, and*

[2]*Department of Plant and Microbial Biology, Howard Hughes Medical Institute, University of California, Berkeley, CA 94720-3102, USA*

Received 1 June 2018; revised 18 June 2018; accepted 25 June 2018.
*For correspondence (e-mails miwai@berkeley.edu, niyogi@berkeley.edu).

SUMMARY

The chloroplast is the chlorophyll-containing organelle that produces energy through photosynthesis. Within the chloroplast is an intricate network of thylakoid membranes containing photosynthetic membrane proteins that mediate electron transport and generate chemical energy. Historically, electron microscopy (EM) has been a powerful tool for visualizing the macromolecular structure and organization of thylakoid membranes. However, an understanding of thylakoid membrane dynamics remains elusive because EM requires fixation and sectioning. To improve our knowledge of thylakoid membrane dynamics we need to consider at least two issues: (i) the live-cell imaging conditions needed to visualize active processes *in vivo*; and (ii) the spatial resolution required to differentiate the characteristics of thylakoid membranes. Here, we utilize three-dimensional structured illumination microscopy (3D-SIM) to explore the optimal imaging conditions for investigating the dynamics of thylakoid membranes in living plant and algal cells. We show that 3D-SIM is capable of examining broad characteristics of thylakoid structures in chloroplasts of the vascular plant *Arabidopsis thaliana* and distinguishing the structural differences between wild-type and mutant strains. Using 3D-SIM, we also visualize thylakoid organization in whole cells of the green alga *Chlamydomonas reinhardtii*. These data reveal that high light intensity changes thylakoid membrane structure in *C. reinhardtii*. Moreover, we observed the green alga *Chromochloris zofingiensis* and the moss *Physcomitrella patens* to show the applicability of 3D-SIM. This study demonstrates that 3D-SIM is a promising approach for studying the dynamics of thylakoid membranes in photoautotrophic organisms during photoacclimation processes.

Keywords: structured illumination microscopy, live-cell imaging, thylakoid structure, technical advance, *Arabidopsis thaliana*, *Chlamydomonas reinhardtii*.

INTRODUCTION

Light energy is essential for photosynthesis, and environmental fluctuations in light conditions affect the biomass and growth of green algae and plants. Regulation of photosynthetic light harvesting is a key component in maintaining efficient photosynthesis under changing light conditions (Horton *et al.*, 1996; Niyogi, 1999; Ruban, 2016; Wobbe *et al.*, 2016). Light energy captured by the light-harvesting complex (LHC) proteins is transferred to two photosystems (PSI and PSII), where their reaction centers undergo charge separation to initiate electron transfer (Nelson, 2011). The different macrostructures comprising photosystems and their associated LHC proteins affect the rate of excitation energy transfer (Caffarri *et al.*, 2011; Valkunas *et al.*, 2011). Under fluctuating light conditions, rearrangements of LHC proteins and their connections with photosystems occur to fine-tune the photochemical reactions (Betterle *et al.*, 2009; Wientjes *et al.*, 2013). Such rearrangements cause changes in the macro-organization of thylakoid membrane structures (Johnson *et al.*, 2011; Goral *et al.*, 2012; Kouril *et al.*, 2013; Wood *et al.*, 2018).

Multiple different transcriptional and post-translational levels of regulation are involved in such photoacclimation mechanisms (Rochaix, 2014; Erickson *et al.*, 2015). However, due to the technical limitations required to visualize such intraorganellar membranes *in vivo*, it is not known how the dynamic reorganization of the macrostructure involving photosystems and their LHC proteins is regulated in thylakoid membranes.

Recent advances in cryo-electron tomography (cryo-ET) (Beck and Baumeister, 2016) have enabled *in vivo* volumetric visualization of thylakoid membranes. The reconstructed three-dimensional (3D) thylakoid structures of vascular plants derived from cryo-ET, obtained using serial sections of stained chloroplasts that are cryo-immobilized and dehydrated by freeze substitution, reveal a unique branching structure connecting grana (stacked membrane regions) and stroma lamellae (non-stacked membrane regions) (Shimoni *et al.*, 2005; Austin and Staehelin, 2011). Under increased light conditions, cryo-ET of unstained *Arabidopsis thaliana* leaves shows light-induced expansion in the lumenal space of grana, suggesting that diffusion in the lumen is increased under light conditions (Kirchhoff *et al.*, 2011). Recently, a combination of cryo-ET and a cryo-focused ion beam to obtain thin cryo-sections was successful in generating the first 3D thylakoid structures of the unicellular green alga *Chlamydomonas reinhardtii* (Engel *et al.*, 2015). This reconstruction details the membrane characteristics in the cup-shaped chloroplast, including the convergent membrane tip pointing toward the chloroplast envelope and the tubular membranes around and inside the pyrenoid (Engel *et al.*, 2015). Although electron microscopy (EM) provides sufficient spatial resolution to distinguish thylakoid membranes and the lumenal space, major drawbacks are that the samples need to be fixed and sectioned, making it impossible to observe dynamic behaviors occurring within a whole chloroplast in its native state.

Confocal laser scanning microscopy provides the ability to observe dynamic and native behaviors in live cells, but compromises higher spatial resolution. Because thylakoid membranes contain chlorophyll (Chl)-binding proteins, it is simple to observe Chl fluorescence in thylakoid membranes without staining or expressing transgenic fluorescent proteins. However, it is difficult to obtain clear images of the thylakoid structure within chloroplasts using a conventional microscope because of the high abundance of Chl pigments in thylakoid membranes. Thylakoid membranes form intricate networks of grana and stroma lamellae structures that are about 5–10 μm in size. It is possible to visualize thylakoid membranes in the moss *Physcomitrella patens* with increased spatial resolution by using 3D image deconvolution processing and determining photon-emitting positions through reverse calculation of the convolved point spread function (Iwai *et al.*, 2014, 2016). In this study, we applied 3D structured illumination microscopy (3D-SIM) to characterize thylakoid membranes in chloroplasts of *A. thaliana* and *C. reinhardtii* at subdiffraction resolution. Structured illumination microscopy provides the ability to achieve lateral resolution beyond the diffraction limit by the excitation of laterally defined patterned light ('structured illumination') in a widefield microscope. Application of 3D imaging by obtaining the axial information enhances the resolution to 100–130 nm in the lateral dimension and 280–350 nm in the axial dimension (Gustafsson *et al.*, 2008). Our results suggest that 3D-SIM is capable of differentiating overall thylakoid characteristics caused by different growing light conditions and in different mutant lines. This study provides proof of principle that 3D-SIM can be exploited to understand dynamic behaviors of thylakoid membranes in live cells.

RESULTS

Differentiating *in vivo* thylakoid characteristics in whole *A. thaliana* chloroplasts using 3D-SIM

In this study we used a commercially available Carl Zeiss Elyra PS.1 SIM (see Experimental Procedures for details). Chlorophyll fluorescence can be used to visualize thylakoid structures because Chl-binding membrane proteins are abundantly distributed throughout thylakoid membranes. We observed chloroplasts in the mesophyll tissues of *A. thaliana* wild-type (WT) leaves. Because of the numerous Chl pigments in thylakoid membranes, Chl fluorescence intensity in the widefield images was too high to distinguish actual signals from background noise (Figure 1a). This common problem prevents visualization of fine thylakoid membrane structures. To obtain subdiffraction resolution of a fluorescence image, 3D-SIM requires acquisition of multiple images with the excitation of structured illumination having three to five phase shifts at three to five different angles (Demmerle *et al.*, 2017). The final image is reconstructed via post-processing with mathematical algorithms. In the reconstructed 3D-SIM image, each granum within the chloroplast was clearly visible by Chl fluorescence (Figure 1b).

To examine if 3D-SIM is capable of differentiating structural differences in thylakoids, we compared the *in vivo* grana size of *A. thaliana* WT and specific mutant lines. *In vivo* grana size was determined by measuring the full-width at the half maximum (FWHM; the distance between points on the Gaussian distribution where the value is half of its peak value) of grana Chl fluorescence from reconstructed 3D-SIM images with subdiffraction resolution. We used the mutant lines *stn7 stn8* and *tap38*, which possess a larger and smaller grana size, respectively, when observed by EM (Fristedt *et al.*, 2009;

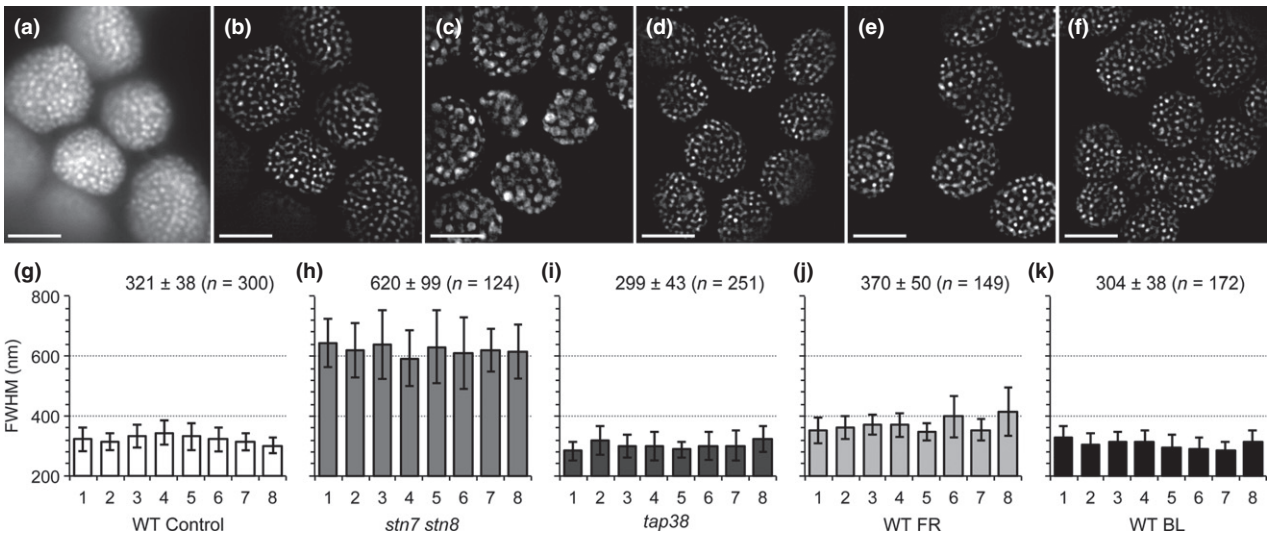

Figure 1. Subdiffraction-resolution live-cell imaging analysis of the grana size of *Arabidopsis thaliana* chloroplasts.
Chlorophyll fluorescence from *A. thaliana* chloroplasts in the mesophyll tissue observed and analyzed by three-dimensional structured illumination microscopy (3D-SIM). Compared with the reconstructed widefield image (a), the reconstructed 3D-SIM image (b) of chloroplasts in the wild type (WT) showed distinct round structures, indicating the individual grana. The reconstructed 3D-SIM images of chloroplasts in (b) the WT control, (c) the *stn7 stn8* mutant, (d) the *tap38* mutant, and the WT acclimated to (e) far-red (FR) light and (f) blue light (BL) conditions were analyzed to measure the differences in grana size. Scale bars = 5 μm. The full width at half maximum (FWHM) of grana from (g) the WT control (n = 300 from eight chloroplasts), (h) the *stn7 stn8* mutant (n = 124 from eight chloroplasts), (i) the *tap38* mutant (n = 251 from eight chloroplasts), and the WT chloroplasts acclimated to (j) FR light (n = 149 from eight chloroplasts) or (k) BL (n = 172 from eight chloroplasts). Inset numbers indicate mean FWHM ± SD of all chloroplasts, and data represent means ± SD for each chloroplast.

Armbruster *et al.*, 2013). For eight chloroplasts in the mesophyll tissues of the WT and both mutants, we measured FWHM of all clearly defined grana in each chloroplast (Figure 1b–d). The WT had a grana FWHM of 321 ± 38 nm (Figure 1g; n = 300 from eight chloroplasts). By comparison, the grana FWHM of *stn7 stn8* mutant was 620 ± 99 nm (Figure 1h; n = 124 from eight chloroplasts), which was roughly twice as large as that of the *tap38* mutant, at 299 ± 43 nm (Figure 1i; n = 251 from eight chloroplasts). Such a large difference was previously observed by EM (Armbruster *et al.*, 2013). We also observed that the number of grana present within *stn7 stn8* was about half that in the *tap38* mutant, which suggests that the total volume of thylakoid membranes may be the same in the two mutants. While these results showed minimal variation of grana size within an individual chloroplast and among chloroplasts, this technique provides the ability to quantify these characteristics.

To test whether 3D-SIM can differentiate structural characteristics of thylakoids caused by different light conditions, we observed grana from WT *A. thaliana* acclimated to far-red (FR) or blue (BL) light for 2 h (Figure 1e,f), conditions known to induce dephosphorylation or phosphorylation of LHC proteins of PSII (LHCII) by TAP38/PPH1 phosphatase (Pribil *et al.*, 2010; Shapiguzov *et al.*, 2010) or STN7 kinase (Bellafiore *et al.*, 2005), respectively. These results indicated that the FWHM of FR- and BL-acclimated grana was 370 ± 50 nm (Figure 1j; n = 149 from eight chloroplasts) and 304 ± 38 nm (Figure 1k; n = 172 from eight chloroplasts), respectively. The BL-acclimated chloroplasts showed similar average FWHM to the *tap38* mutant, because BL acclimation and *tap38* are both known to promote phosphorylation of LHCII (Haldrup *et al.*, 2001; Pribil *et al.*, 2010; Shapiguzov *et al.*, 2010). In contrast, the grana of FR-acclimated chloroplasts were not as large as in the *stn7 stn8* mutant, most likely because FR light does not have a major effect on the dephosphorylation of PSII core proteins, which involves STN8 kinase, whereas the *stn7 stn8* mutant shows almost complete dephosphorylation of both LHCII and PSII core proteins (Bonardi *et al.*, 2005). Although there were variations among different chloroplasts, the difference between BL- and FR-acclimated grana size observed by 3D-SIM was statistically significant (Student's t-test, $P < 0.0001$).

In mesophyll chloroplasts of *A. thaliana* leaves the grana stacks are usually oriented perpendicular to the leaf surface (Figure 1). While a side view of thylakoid structures is rarely observable *in vivo*, it is possible to image this view by 3D-SIM using isolated intact chloroplasts. To visualize the side view of chloroplasts by 3D-SIM we resuspended isolated intact chloroplasts in low-melting-point agarose medium, which embedded and immobilized chloroplasts in a random orientation. The reconstructed 3D-SIM images show the side view of whole isolated chloroplasts in which the layered membrane structures of the grana are visible

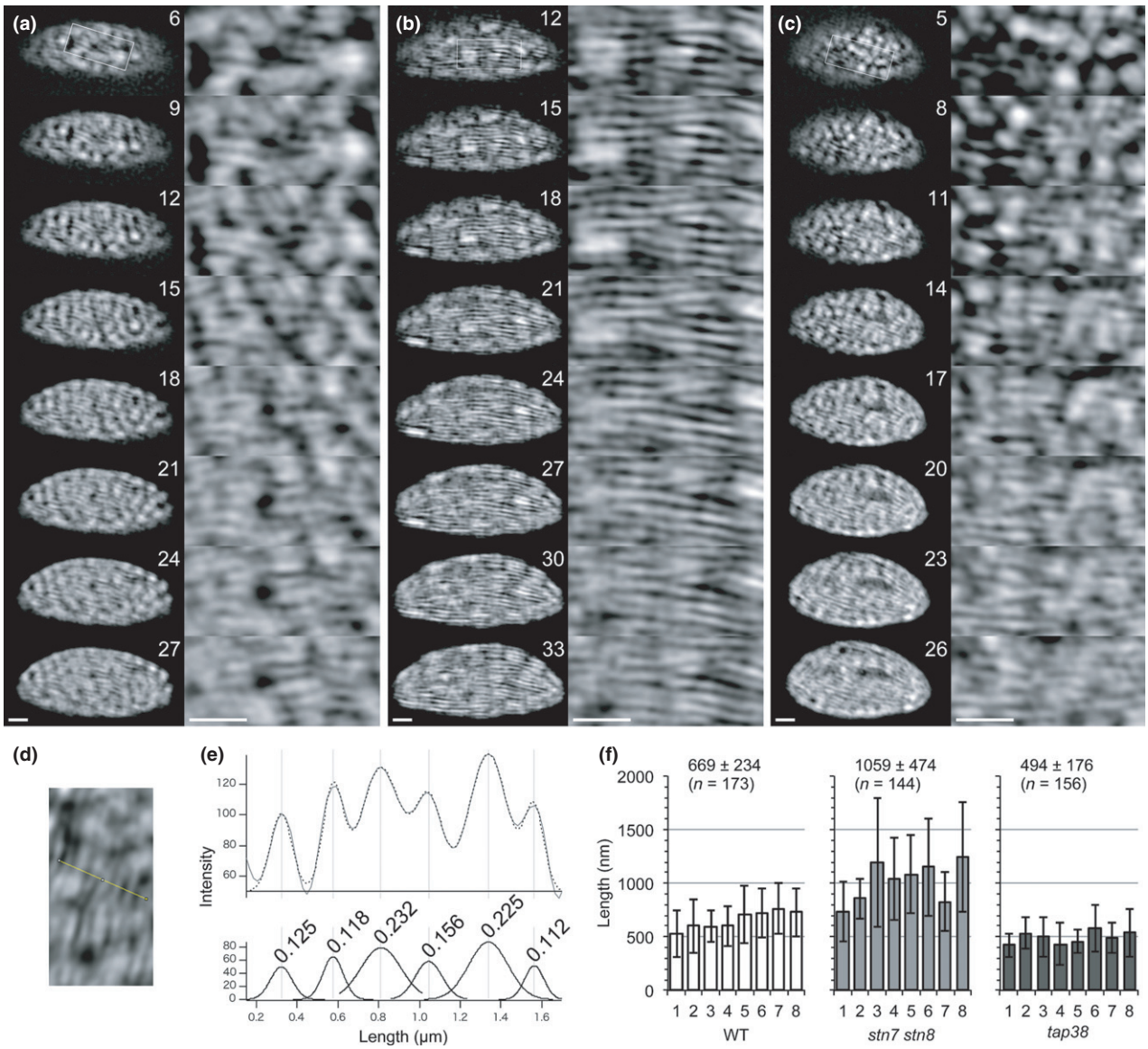

Figure 2. Reconstructed three-dimensional structured illumination microscopy (3D-SIM) images of the side view of *Arabidopsis thaliana* chloroplasts showing the thylakoid membrane architecture.

Chlorophyll fluorescence from isolated *A. thaliana* chloroplasts observed by 3D-SIM. Optical sections of chloroplasts isolated from (a) the wild type (WT), (b) *stn7 stn8*, and (c) *tap38* are shown whole (left column) and enlarged to show detail (right column). Each number corresponds to the selected focal plane of the serial optical sections as shown in Figures S1–S3. Scale bars = 1 μm. (d) Representative close-up image of a chloroplast side view with a line scan for a thickness analysis of thylakoid membranes. (e) The intensity profile of the line indicated in (d) (top panel). The dotted line is the multipeak fit, which is used to extract the Gaussian distribution of each peak (bottom panel). The numbers indicate full width at half maximum (FWHM) (in μm) measured in each Gaussian distribution. (f) Thylakoid membrane length in chloroplasts of WT (n = 173 from eight chloroplasts), *stn7 stn8* (n = 144 from eight chloroplasts) and *tap38* (n = 156 from eight chloroplasts). Inset numbers indicate mean FWHM ± SD of all chloroplasts, and data represent means ± SD for each chloroplast. [Colour figure can be viewed at wileyonlinelibrary.com].

(Figure 2a–c). This orientation is similar to what is usually observed by EM in chemically or cryogenically fixed and sectioned leaves. However, because light microscopy is capable of optical sectioning through samples it is possible to analyze the membrane structures through the whole chloroplast in a non-destructive way with 3D-SIM (Figures S1–S3 in the online Supporting Information). We measured the thickness of each layer of thylakoid membranes from reconstructed 3D-SIM images (Figure 2d, e). The FWHM of each layer was similar in the WT and the two mutants [WT, 131 ± 27 nm (n = 27 from five chloroplasts); *stn7 stn8*, 133 ± 23 nm (n = 30 from five chloroplasts); *tap38*, 119 ± 24 nm (n = 29 from five chloroplasts)]. The thinnest FWHM observed was 85 nm. A previous cryo-EM study (Kirchhoff *et al.*, 2011) found that the stacking repeat distance (i.e. the thickness of two

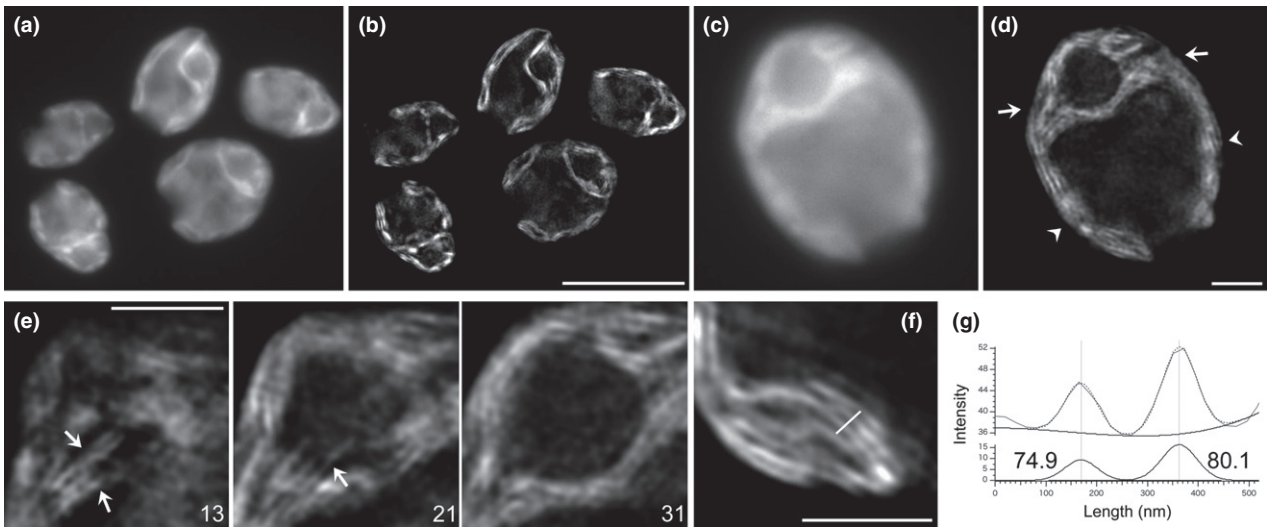

Figure 3. Subdiffraction-resolution live-cell imaging analysis of *Chlamydomonas reinhardtii* chloroplasts.
Chlorophyll fluorescence from *C. reinhardtii* chloroplasts observed by three-dimensional structured illumination microscopy (3D-SIM). Compared with reconstructed widefield images (a, c), reconstructed 3D-SIM images (b, d) of *C. reinhardtii* chloroplasts reveal the distinct thylakoid membrane structures. Arrows and arrowheads in (d) indicate the basal and lobe regions, respectively. (e) Selected optical sections of close-up 3D-SIM images showing the basal region of the chloroplast shown in (d). Each number corresponds to the selected focal plane of the serial optical sections as shown in Figure S4. Arrows in (e) indicate thylakoid membranes, which appeared to extend into the pyrenoid. (f) Detailed image of the thylakoid tip convergence region. (g) The intensity profile of the line indicated in (f). The dotted line is the multipeak fit, which was used to extract the Gaussian distribution of each peak as shown at the bottom. The number indicates the full width at half maximum (in nm) measured in each Gaussian distribution. Scale bars = 10 μm (a, b), 2 μm (c–f).

thylakoid membrane bilayers, the lumen and a stromal gap between appressed membrane bilayers) of *A. thaliana* grana thylakoids is 15.7–16.3 nm under normal conditions. Using the reported stacking repeat distance, the thinnest layer we observed (85 nm) could contain at most five grana disks. Because of this limitation in spatial resolution it is not practical to quantify the thickness of grana stacks, although the overall side view of chloroplasts showed thylakoid membrane structures that appeared to include grana and stroma lamellae (Figure 2a–c).

Comparing the overall side view of chloroplasts from the WT, *stn7 stn8* mutant and *tap38* mutant showed differences in apparent membrane lengths (from one edge to the other of a clearly defined membrane) (Figure 2a–c). We used ImageJ software to measure the length of membranes, and these results indicated that the *stn7 stn8* mutant had the longest membranes (Figure 2f). While there was minimal variation among chloroplasts of the same genotype, this technique enables quantification of the differences in thylakoid membrane length between genotypes (Figure 2f). Although the differences appear small, the membrane length of *tap38* chloroplasts is statistically shorter than the WT membrane (Figure 2f; Student's *t*-test, $P < 0.001$). These results are similar to the quantifications of grana diameter in the *stn7 stn8* and the *tap38* chloroplasts (Figure 1c,e), suggesting that 3D-SIM is capable of visualizing the traditional side view of chloroplasts in a non-destructive way that maintains the native conditions observed *in vivo*.

In vivo visualization of the characteristics and structural dynamics of thylakoid membranes in whole cells of *C. reinhardtii* using 3D-SIM

To assess the capabilities of 3D-SIM in algae we imaged thylakoid membranes of the model unicellular green alga *C. reinhardtii.* To minimize cellular movements caused by flagellar activity, we embedded live cells of *C. reinhardtii* in low-melting-point agarose medium (see Experimental Procedures for details). Similar to what we observed with *A. thaliana* chloroplasts, the Chl fluorescence intensity of widefield images was too high to distinguish the thylakoid structures in the cells (Figure 3a,c). After reconstructing 3D-SIM images, the thylakoid membrane structures were revealed (Figures 3b,d and S4). Our 3D-SIM reconstructions confirm broadly appressed thylakoid membrane regions in *C. reinhardtii* chloroplasts as reported in the literature, which contrasts with the distinct grana structure observed in vascular plants (as shown in Figure 1). Optical sectioning showed that membrane structures extend into the pyrenoid (Figure 3e, arrows), verifying previous observations by cryo-ET (Engel *et al.*, 2015) and confocal microscopy (Mackinder *et al.*, 2017). We also observed the thylakoid tip convergence region (Figure 3f), as described in cryo-ET images (Engel *et al.*, 2015) and measured the thickness of each membrane region observed using reconstructed 3D-SIM images. The average thickness of each layer was 124.0 ± 20.3 nm ($n = 38$) (Figure 3f,g), but the thinnest membrane region was 74.9 nm. The stacking

repeat distance of *C. reinhardtii* thylakoids, as determined by cryo-ET, was 22.4 ± 1.3 nm (Engel *et al.*, 2015). Using the reported stacking repeat distance, it is likely that the thinnest layer we observed (Figure 3f,g) contained three or fewer layers of stacked thylakoids.

Optical sectioning through the whole chloroplast enabled us to investigate unique thylakoid membrane structures in the cup-shaped chloroplast in *C. reinhardtii* (Figure 3). We used similar methods to those in our 3D-SIM analyses of *A. thaliana* (as shown in Figure 2). We reconstructed 3D-SIM images from *C. reinhardtii* cells grown photoautotrophically and heterotrophically under dim light conditions (DL; about 5 μmol photons m^{-2} sec^{-1}). We observed a wide variety of thylakoid membrane structures and overall appearances in different cells from the same condition (Figure 4a,b). By adjusting the focal plane to near the cell surface, we could observe the membrane surface patterns, which are usually difficult to obtain by EM observation. The reconstructed 3D-SIM images revealed randomly shaped membrane surface patterns which showed continuous membrane regions with occasional empty spaces (Figure 4a,b). It is apparent that the size, shape and location of empty spaces on membranes are not uniformly arranged. Such random patterns of empty spaces make the membrane organization observed at the central focal planes appear different in each cell. Surprisingly, we did not observe apparent differences in membrane structures between photoautotrophically and heterotrophically grown cells under DL despite reported differences in photosynthesis and light harvesting (Heifetz *et al.*, 2000).

Intriguingly, 3D-SIM observations revealed that many *C. reinhardtii* cells grown photoautotrophically under low-light conditions (LL; about 50 μmol photons m^{-2} sec^{-1}) had patchy membrane surface patterns (Figure 4c, slice numbers 1–10). Moreover, after 1 day's growth under high light conditions (HL; about 350 μmol photons m^{-2} sec^{-1}), many *C. reinhardtii* cells lacked partial or whole lobes (the regions extending from the base of the cup-shaped chloroplast toward the flagella at the anterior of the cell; Figure 4d). Under HL, the patchy membrane surface patterns became unclear due to the loss of the lobes. However, we observed the recovery of the lobes within 1 day of returning the cells to LL conditions (Figure S5a). We also observed a similar lobe shrinking phenotype in the *npq4 lhcsr1* mutant, which lacks qE type mechanisms of non-photochemical quenching (NPQ), grown photoautotrophically under HL (Figure S5b) (Ballottari *et al.*, 2016). This result suggests that the lobe shrinking process is independent of qE mechanisms. It has been suggested that the lobe region contains photosynthetically active thylakoid membranes with fully assembled PSII–LHCII supercomplexes, while the basal region contains biogenic membranes where protein synthesis and membrane biogenesis

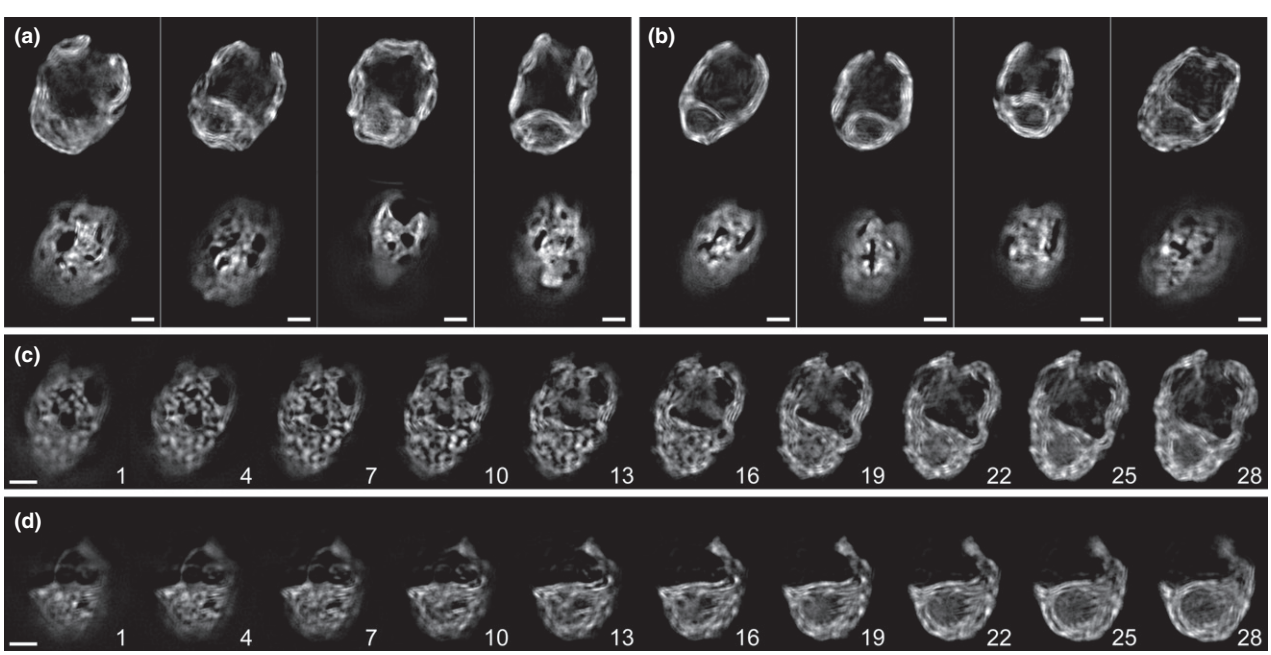

Figure 4. Structural comparison of thylakoid structures in *Chlamydomonas reinhardtii* cells grown under different conditions.
Chlorophyll (Chl) fluorescence from chloroplasts of *C. reinhardtii* observed by three-dimensional structured illumination microscopy (3D-SIM). Reconstructed 3D-SIM images of Chl fluorescence showing paired central (top image) and peripheral (bottom image) focal planes of (a) heterotrophically and (b) photoautotrophically grown cells under dim light conditions (about 5 μmol photons m^{-2} sec^{-1}). Optical sections from the peripheral to central focal planes of photoautotrophically grown cells under (c) low light (about 50 μmol photons m^{-2} sec^{-1}) and (d) high light (about 350 μmol photons m^{-2} sec^{-1}) conditions. The numbers indicate selected focal planes of the optical sections. Scale bars = 2 μm.

take place (Schottkowski *et al.*, 2012). We hypothesize that the shrinking of thylakoid membranes at the lobe region decreases light absorption under HL and could prevent immediate photodamage from occurring at the basal region.

Visualizing other organelles and photosynthetic organisms using 3D-SIM

Using chemical labeling techniques, SIM is readily capable of visualizing non-fluorescent organelles. For example, we used MitoTracker (MT) to stain mitochondria in *C. reinhardtii*; these are known to change morphology during the life cycle. We stained and observed cells grown heterotrophically under DL. Reconstructed 3D-SIM images confirmed the tubular structure of the mitochondrial network (Figure 5a) that has been frequently observed at the end of the light period during the day/night cycle (Ehara *et al.*, 1995). Optical sectioning of reconstructed 3D-SIM images indicated that the tubular mitochondrial structure was continuous and located close to the surface of the chloroplast (Figure 5c). Furthermore, we used BODIPY to stain neutral lipids in the *C. reinhardtii* cells under nitrogen starvation. The reconstructed 3D-SIM images showed the formation of neutral lipid droplets located in close proximity to the chloroplast envelope (Figure 5b), which is similar to what has been observed by EM (Goodson *et al.*, 2011; Moriyama *et al.*, 2018). However, the location of the lipid droplets makes it difficult to distinguish whether they are in the chloroplast or cytosol. Interestingly, optical sectioning and the reconstructed 3D-SIM images revealed connections between some lipid droplets (Figure 5d). Additionally, under nitrogen starvation conditions, the Chl fluorescence of thylakoid structure and organization was greatly disrupted (Figure 5b). These results suggest that morphological changes in the mitochondrial network and formation of lipid droplets, in conjunction with thylakoid structure and organization, can be visualized at subdiffraction resolution by time-lapse 3D-SIM analysis.

To seek wider applicability of 3D-SIM to other organisms, we investigated the green alga *Chromochloris zofingiensis*. This alga shows increased in accumulation of astaxanthin and lipids under a variety of conditions, including heterotrophy (Mulders *et al.*, 2014; Zhang *et al.*, 2016; Roth *et al.*, 2017). Staining heterotrophic cells with BODIPY and imaging with 3D-SIM revealed cytosolic lipid bodies accumulating near the periphery of the cell (Figure 5e). The reconstructed 3D-SIM images also showed irregular shapes of thylakoid membranes in the heterotrophically grown cell (Figure 5e).

Furthermore, we also tested 3D-SIM with protonemal cells from the moss *P. patens*. We grew *P. patens* protonema on agar medium without or with glucose. Growth of *P. patens* grown without glucose is known to induce chloronemal cells, which contain more chloroplasts, while growth with glucose induces caulonemal cells, which contain fewer chloroplasts (Schumaker and Dietrich, 1997; Olsson *et al.*, 2003). The reconstructed 3D-SIM images showed distinct grana structures in the chloroplasts in the chloronemal cells (Figure 5f), while the chloroplasts in the caulonemal cells did not have well-defined grana structures (Figure 5g). Using MT we observed mitochondria in both types of protonemal cells. The reconstructed 3D-SIM images indicated that mitochondria in the caulonemal cells appeared to be longer and more tubular than those in the chloronemal cells (Figure 5f,g). This change in mitochondrial structure may be correlated with the energy supply, which is known to control the balance between chloronemal and caulonemal cells (Thelander *et al.*, 2005).

DISCUSSION

Chloroplasts are readily observable by fluorescence microscopy as small, distinct and autofluorescent organelles in photosynthetic organisms. However, visualizing and resolving structures inside chloroplasts *in vivo* is challenging because of the bright Chl fluorescence from numerous photosynthetic membrane proteins in the intricate thylakoid membrane structures within an organelle of size 5–10 μm (Figures 1a and 2a,c). In this study, we utilized 3D-SIM to visualize the structural organization of thylakoid membranes in chloroplasts. Our observations demonstrate that 3D-SIM provides the capacity to investigate the detailed network of thylakoid membranes in the chloroplasts of *A. thaliana* and *C. reinhardtii in vivo*. Our results indicate that the spatial resolution of the reconstructed 3D-SIM images is not sufficient to distinguish each individual layer within a stack of thylakoid membranes (15.7 nm for *A. thaliana* and 22.4 nm for *C. reinhardtii* as observed by cryo-ET) (Kirchhoff *et al.*, 2011; Engel *et al.*, 2015). Nevertheless, our results suggest that the differences in thylakoid membrane characteristics in different mutants and under different growth conditions can be distinguished and analyzed in reconstructed 3D-SIM images (Figures 1, 2 and 4). Recently, isolated chloroplasts from spinach have also been observed by 3D-SIM, showing the smaller and larger grana sizes in response to light and dark conditions and caused by phosphorylation and dephosphorylation of LHCII (Wood *et al.*, 2018).

A major advantage of using optical microscopy is that no sample sectioning is necessary to acquire the images, which allows us to observe a wide volumetric range of intact samples via optical serial sectioning. With the subdiffraction spatial resolution achieved by 3D-SIM, it is possible to visualize thylakoid characteristics in a whole chloroplast by a non-destructive method (Figures S1–S4). Our observations indicate that there are structural variations in the characteristics of thylakoids in each chloroplast, even within the same strain under the same conditions (Figures 1g–k, 2f and 4a,b). With 3D-SIM, it is

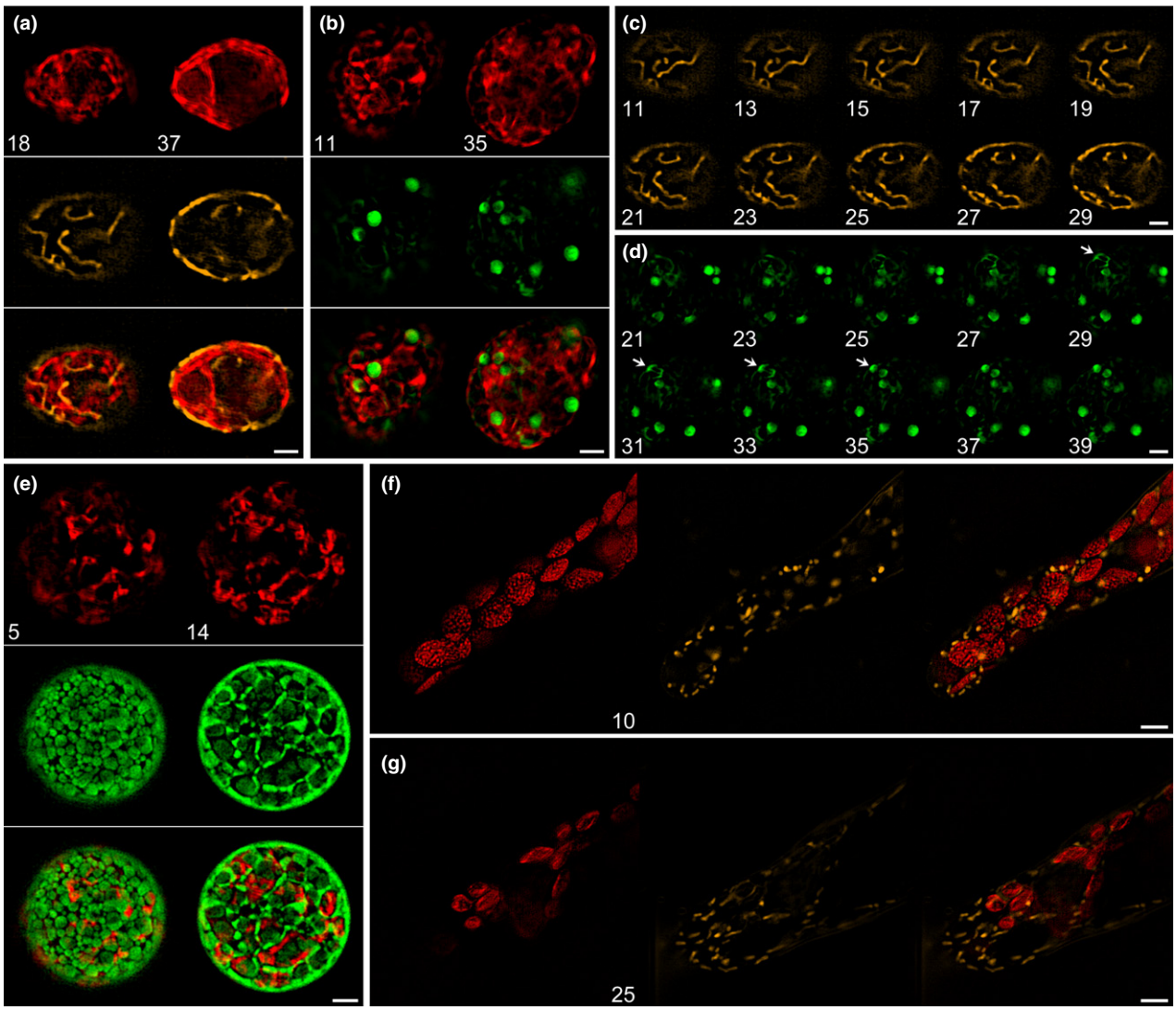

Figure 5. Reconstructed three-dimensional structured illumination microscopy (3D-SIM) images of other organelles and photosynthetic organisms.
(a) The mitochondria in heterotrophically grown *Chlamydomonas reinhardtii* cells were stained by MitoTracker (MT) and observed by 3D-SIM. Top, chlorophyll (Chl); middle, MT; bottom, merged. (b) Lipid droplets in *C. reinhardtii* cells under nitrogen starvation were stained by BODIPY and observed by 3D-SIM. Top, Chl; middle, BODIPY; bottom, merged. (c) MT fluorescence in selected optical sections from the peripheral to central focal planes of the cell as shown in (a). (d) BODIPY fluorescence in the selected optical sections from the peripheral to central focal planes of the cell as shown in (b). Arrows indicate a lipid droplet connecting to another one in the different focal planes. (e) Lipid bodies in heterotrophically grown *Chromochloris zofingiensis* cells were stained by BODIPY and observed by 3D-SIM. Top, Chl; middle, BODIPY; bottom, merged. Mitochondria in (f) chloronemal cells and (g) caulonemal cells of *Physcomitrella patens* were stained by MT and observed by 3D-SIM. Left, Chl; middle, MT; right, merged. Numbers indicate the selected focal planes of the serial optical sections. Scale bars = 2 μm (a–e), 5 μm (f, g).

possible to analyze with statistical support a large number of samples to reveal structural characteristics of thylakoids *in vivo*; this is often too time-consuming for EM. Moreover, EM requires fixing and staining of samples as opposed to the *in vivo* or near native state of chloroplasts used for 3D-SIM. Altogether, this study shows that 3D-SIM is a valuable method for obtaining high-resolution images and analyzing a large number of *in vivo* or near native state chloroplasts to elucidate thylakoid membrane dynamics and more.

It is worth mentioning the drawbacks of using 3D-SIM. To reconstruct a 3D-SIM image at subdiffraction resolution requires at least 15 images to be captured (images excited with five different phase-shifted patterns of light at three different angles of rotation) (Demmerle *et al.*, 2017). With our 3D-SIM system it takes about 10 ms to acquire a raw image of Chl fluorescence (512 × 512 pixels) and roughly 4 sec to acquire a volumetric image containing 10 sequential focal planes with 100-nm *z*-intervals. As is always a concern with laser microscopy observations, a certain level

of photodamage can occur and must be assessed with a series of control experiments when conducting time-lapse 3D-SIM analyses. Also, it is essential to adjust the instrument settings and optimize imaging conditions to avoid artifacts during image reconstruction; these can often occur when fluorescence signals are low and non-modulated noise signals interfere with real structures. The blurred hexagonal repeating signals, in particular outside the main Chl fluorescence signal, of the thylakoid surface membrane structures in *C. reinhardtii* (Figure 4c, slice number 1) are an example of an artifact. This artifact is due not only to the weak signals but also the optical aberration caused by the curved cell surface with different refractive properties. To evaluate the quality of the reconstructed 3D-SIM images, programs such as SIMcheck (Ball *et al.*, 2015) for ImageJ are helpful. It is sometimes impractical to prevent optical aberration from occurring because of the strong Chl fluorescence from an oval shaped object of size 5–10 μm, such as chloroplasts and *C. reinhardtii* cells; therefore, it is also important to evaluate the presence of an artifact by examining each sequential focal plane in a reconstructed 3D-SIM image.

In general, there are several caveats for live-cell imaging of chloroplasts and thylakoid membranes. As mentioned earlier, it is often practical to assume that the structures visualized by Chl fluorescence indicate thylakoid membranes because these are filled with Chl-binding membrane proteins. However, it is important to keep in mind that Chl fluorescence is not emitted directly by the thylakoid membranes themselves. Chlorophyll fluorescence intensity can also be affected by many factors such as induction of NPQ and the redox state of plastoquinone pools in thylakoid membranes. We observed the shrinkage of fluorescent thylakoid structures at the lobe region in *C. reinhardtii* chloroplasts under HL conditions (Figure 4d), but this technique cannot distinguish whether thylakoid membranes have been lost from the lobes or whether they remain but have lost Chl fluorescence emission due to HL stress. 3D-SIM of Chl fluorescence also cannot determine the location of or changes in the chloroplast envelope. Furthermore, it is known that the level of Chl fluorescence emission from PSI is much lower than that from PSII at room temperature. Fluorescence microscopy imaging conditions generally adjust the detection sensitivity to the highest signal (i.e. PSII fluorescence) observed in the field of view. Therefore, when imaging Chl fluorescence at room temperature without spectral and/or fluorescence lifetime imaging, PSI fluorescence is often nearly invisible in the acquired images. However, the benefits of 3D-SIM and its capacity to visualize whole chloroplasts *in vivo* at high resolution offer possibilities to provide insights into the dynamics of thylakoid membranes.

CONCLUSION

Observations of chloroplast membrane structure at high spatial resolution *in vivo* will improve our understanding of thylakoid membrane dynamics. This study demonstrates the capacity of 3D-SIM to differentiate general thylakoid membrane characteristics using non-destructive techniques. These findings could be applied in future studies to investigate thylakoid membrane dynamics. Technological improvements in 3D-SIM could enable visualization of individual layers of thylakoid membranes. In addition to the subdiffraction spatial resolution provided by 3D-SIM, increased temporal resolution (Chen *et al.*, 2014; Hayashi and Okada, 2015) will also be essential to further explore thylakoid dynamics. Moreover, developments in deconvolution algorithms to reconstruct accurate images with very low signals (Arigovindan *et al.*, 2013) will be critical to reduce phototoxicity for time-lapse imaging. Development of imaging techniques to visualize thylakoid dynamics will provide not only an understanding of the regulation of photosynthesis at unprecedented spatiotemporal scales but also expand the possibilities for investigating other molecular activities occurring in the chloroplasts of photosynthetic organisms.

EXPERIMENTAL PROCEDURES

Strains and growth conditions

Arabidopsis thaliana WT (ecotype Columbia-0), *stn7 stn8* (Fristedt *et al.*, 2009) and *tap38* (Pribil *et al.*, 2010) were grown on soil under about 100 μmol photons m^{-2} sec^{-1} with light (10 h) and dark (14 h) cycles at 21°C for 4–5 weeks. *Chlamydomonas reinhardtii* WT (4A+) (Dent *et al.*, 2005) was grown either photoautotrophically in minimal HS liquid medium or heterotrophically in acetate-containing TAP liquid medium under continuous LL conditions (about 50 μmol photons m^{-2} sec^{-1}) as described previously (Baroli *et al.*, 2004). Different light treatments included continuous DL (about 5 μmol photons m^{-2} sec^{-1}) and continuous HL (about 350 μmol photons m^{-2} sec^{-1}) conditions. For nitrogen starvation conditions the culture at mid-exponential growth phase in TAP liquid medium was transferred to medium without a nitrogen source and grown under LL conditions for 3 days. *Chromochloris zofingiensis* WT (SAG 211-14) was grown heterotrophically in Proteose medium (UTEX Culture Collection of Algae, https://utex.org/) with Chu's micronutrient solution and 10 mM glucose under about 100 μmol photons m^{-2} sec^{-1} with light (16 h) and dark (8 h) cycles at 25°C as described previously (Roth *et al.*, 2017). *Physcomitrella patens* WT (Gransden 2004) protonema were grown on a layer of cellophane overlaid on BCDAT agar medium without or with glucose (5 g L^{-1}) (Nishiyama *et al.*, 2000) at 25°C under continuous light at about 50 μmol photons m^{-2} sec^{-1}.

Sample preparation for 3D-SIM

The chloroplasts in *A. thaliana* mesophyll tissues (Figure 1) were observed by removing the lower epidermal tissues using tape. The leaf tissues were covered with water placed between two coverslips attached in an Attofluor cell chamber (Thermo Fisher Scientific, https://www.thermofisher.com/). To observe the side view of chloroplasts (Figure 2), chloroplasts were isolated from

A. thaliana leaves as previously described (Mizusawa *et al.*, 1999), except that 40% Percoll was only used to sediment the intact chloroplasts at 3000***g*** for 5 min for quick purification. The intact chloroplasts in the pellet, washed once with 0.03 M HEPES (pH 7.8) and 0.33 M sorbitol at 3000***g*** for 5 min, were resuspended with the 0.5% low-melting-point agarose in Murashige and Skoog medium and mounted between two coverslips placed in an Attofluor cell chamber for 3D-SIM observation. To prepare *C. reinhardtii* cells for microscopy (Figures 3 and 4), the cultures grown under designated conditions were centrifuged at 3000***g*** and 24°C for 1 min. The pelleted cells were resuspended with 0.5% low-melting-point agarose in an appropriate medium (TAP or HS) and mounted between two coverslips placed in an Attofluor cell chamber for 3D-SIM observation. For staining the mitochondria in *C. reinhardtii* (Figure 5a,c), the pelleted cells were resuspended with TAP liquid medium containing 1 μM MitoTracker Orange CMTMRos (Thermo Fisher Scientific). The cells were incubated in the dark for 30 min, and washed three times with TAP liquid medium without dye under the same centrifuge conditions as above. For staining neutral lipids in *C. reinhardtii* cells under nitrogen starvation (Figure 5b,d), the pelleted cells were resuspended with TAP liquid medium without a nitrogen source and containing 5 μg ml^{-1} BODIPY™ 493/503 dye (Thermo Fisher Scientific). The cells were incubated in the dark for 10 min, and washed with TAP liquid medium without dye three times under the same centrifuge conditions as above. For staining neutral lipids in the *C. zofingiensis* cells under heterotrophic growth conditions (Figure 5e), the same BODIPY staining protocol as for *C. reinhardtii* was used, except that Proteose liquid medium was used instead of TAP. To stain the mitochondria in *P. patens* cells (Figure 5f,g), protonema grown on BCDAT agar medium with or without glucose were incubated with 0.5 μM MitoTracker Orange CMTMRos in the dark for 30 min. The protonemal cells were then washed with 5 ml of water and mounted directly on a coverslip.

3D-SIM

The microscopy samples were observed using an Elyra PS.1 SIM microscope (Zeiss, https://www.zeiss.com/) with an alpha Plan-Apochromat 100×/1.46 oil objective lens. Chlorophyll, MT and BODIPY were excited with 642-, 561- and 488-nm lasers, respectively, and fluorescence was acquired through a 655-nm longpass filter, a 570–620-nm bandpass filter and a 495–550-nm bandpass filter, respectively. Image acquisition was done under the full control of ZEN software (Zeiss). One focal plane for each 3D-SIM image was obtained by acquisition of sequential fluorescence images via excitation with patterned light of three rotation angles, each of which contained five phase shifts. The *z*-interval distance was 101 nm. Raw images were processed to reconstruct 3D images with ZEN software. Extraction of the intensity data from each focal plane was performed using the SIMcheck plugin (Ball *et al.*, 2015) for ImageJ software (US National Institutes of Health, https://www.nih.gov/). Peak fitting and FWHM measurements were done using the multipeak fit analysis packages in Igor Pro software (WaveMetrics, https://www.wavemetrics.com/).

ACKNOWLEDGEMENTS

We thank Drs Denise Schichnes and Steven E. Ruzin for the technical setup and maintenance of the Carl Zeiss Elyra PS.1 SIM, which was supported in part by the National Institutes of Health S10 program 1S10OD018136-01. This work was supported by the US Department of Energy, Office of Science, through the Photosynthetic Systems program in the Office of Basic Energy Sciences. The experiments with *C. zofingiensis* were supported by the US Department of Energy, Office of Science, Office of Biological and Environmental Research, under award number DE-SC0018301. KKN is an investigator of the Howard Hughes Medical Institute.

CONFLICT OF INTEREST

The authors declare no conflicts of interest.

SUPPORTING INFORMATION

Additional Supporting Information may be found in the online version of this article.

Figure S1. Optical sections of reconstructed three-dimensional structured illumination microscopy images of the side view of the chloroplast isolated from wild-type *Arabidopsis thaliana* leaves.

Figure S2. Optical sections of reconstructed three-dimensional structured illumination microscopy images of the side view of the chloroplast isolated from *Arabidopsis thaliana stn7 stn8* mutant leaves.

Figure S3. Optical sections of reconstructed three-dimensional structured illumination microscopy images of the side view of the chloroplast isolated from *Arabidopsis thaliana tap38* mutant leaves.

Figure S4. Optical sections of reconstructed three-dimensional structured illumination microscopy images of a wild-type *Chlamydomonas reinhardtii* cell.

Figure S5. Additional reconstructed three-dimensional structured illumination microscopy images showing shrinkage of thylakoid membranes at the lobe region of *Chlamydomonas reinhardtii* chloroplasts under high-light conditions for 1 day.

REFERENCES

Arigovindan, M., Fung, J.C., Elnatan, D., Mennella, V., Chan, Y.H., Pollard, M., Branlund, E., Sedat, J.W. and Agard, D.A. (2013) High-resolution restoration of 3D structures from widefield images with extreme low signal-to-noise-ratio. *Proc. Natl Acad. Sci. USA*, **110**, 17344–17349.

Armbruster, U., Labs, M., Pribil, M. *et al.* (2013) *Arabidopsis* CURVATURE THYLAKOID1 proteins modify thylakoid architecture by inducing membrane curvature. *Plant Cell*, **25**, 2661–2678.

Austin, J.R. 2nd and Staehelin, L.A. (2011) Three-dimensional architecture of grana and stroma thylakoids of higher plants as determined by electron tomography. *Plant Physiol.* **155**, 1601–1611.

Ball, G., Demmerle, J., Kaufmann, R., Davis, I., Dobbie, I.M. and Schermelleh, L. (2015) SIMcheck: a toolbox for successful super-resolution structured illumination microscopy. *Sci. Rep.* **5**, 15915.

Ballottari, M., Truong, T.B., De Re, E., Erickson, E., Stella, G.R., Fleming, G.R., Bassi, R. and Niyogi, K.K. (2016) Identification of pH-sensing sites in the light harvesting complex stress-related 3 protein essential for triggering non-photochemical quenching in *Chlamydomonas reinhardtii*. *J. Biol. Chem.* **291**, 7334–7346.

Baroli, I., Gutman, B.L., Ledford, H.K., Shin, J.W., Chin, B.L., Havaux, M. and Niyogi, K.K. (2004) Photo-oxidative stress in a xanthophyll-deficient mutant of *Chlamydomonas*. *J. Biol. Chem.* **279**, 6337–6344.

Beck, M. and Baumeister, W. (2016) Cryo-electron tomography: can it reveal the molecular sociology of cells in atomic detail? *Trends Cell Biol.* **26**, 825–837.

Bellafiore, S., Barneche, F., Peltier, G. and Rochaix, J.D. (2005) State transitions and light adaptation require chloroplast thylakoid protein kinase STN7. *Nature*, **433**, 892–895.

Betterle, N., Ballottari, M., Zorzan, S., de Bianchi, S., Cazzaniga, S., Dall'osto, L., Morosinotto, T. and Bassi, R. (2009) Light-induced dissociation of an antenna hetero-oligomer is needed for non-photochemical quenching induction. *J. Biol. Chem.* **284**, 15255–15266.

Bonardi, V., Pesaresi, P., Becker, T., Schleiff, E., Wagner, R., Pfannschmidt, T., Jahns, P. and Leister, D. (2005) Photosystem II core phosphorylation and photosynthetic acclimation require two different protein kinases. *Nature*, **437**, 1179–1182.

Caffarri, S., Broess, K., Croce, R. and van Amerongen, H. (2011) Excitation energy transfer and trapping in higher plant photosystem II complexes with different antenna sizes. *Biophys. J.* **100**, 2094–2103.

Chen, B.C., Legant, W.R., Wang, K. *et al.* (2014) Lattice light-sheet microscopy: imaging molecules to embryos at high spatiotemporal resolution. *Science*, **346**, 1257998.

Demmerle, J., Innocent, C., North, A.J., Ball, G., Muller, M., Miron, E., Matsuda, A., Dobbie, I.M., Markaki, Y. and Schermelleh, L. (2017) Strategic and practical guidelines for successful structured illumination microscopy. *Nat. Protoc.* **12**, 988–1010.

Dent, R.M., Haglund, C.M., Chin, B.L., Kobayashi, M.C. and Niyogi, K.K. (2005) Functional genomics of eukaryotic photosynthesis using insertional mutagenesis of *Chlamydomonas reinhardtii*. *Plant Physiol.* **137**, 545–556.

Ehara, T., Osafune, T. and Hase, E. (1995) Behavior of mitochondria in synchronized cells of *Chlamydomonas reinhardtii* (Chlorophyta). *J. Cell Sci.* **108**, 499–507.

Engel, B.D., Schaffer, M., Kuhn Cuellar, L., Villa, E., Plitzko, J.M. and Baumeister, W. (2015) Native architecture of the Chlamydomonas chloroplast revealed by in situ cryo-electron tomography. *eLife*, **4**, e04889.

Erickson, E., Wakao, S. and Niyogi, K.K. (2015) Light stress and photoprotection in *Chlamydomonas reinhardtii*. *Plant J.* **82**, 449–465.

Fristedt, R., Willig, A., Granath, P., Crevecoeur, M., Rochaix, J.D. and Vener, A.V. (2009) Phosphorylation of photosystem II controls functional macroscopic folding of photosynthetic membranes in *Arabidopsis*. *Plant Cell*, **21**, 3950–3964.

Goodson, C., Roth, R., Wang, Z.T. and Goodenough, U. (2011) Structural correlates of cytoplasmic and chloroplast lipid body synthesis in *Chlamydomonas reinhardtii* and stimulation of lipid body production with acetate boost. *Eukaryot. Cell*, **10**, 1592–1606.

Goral, T.K., Johnson, M.P., Duffy, C.D., Brain, A.P., Ruban, A.V. and Mullineaux, C.W. (2012) Light-harvesting antenna composition controls the macrostructure and dynamics of thylakoid membranes in Arabidopsis. *Plant J.* **69**, 289–301.

Gustafsson, M.G., Shao, L., Carlton, P.M., Wang, C.J., Golubovskaya, I.N., Cande, W.Z., Agard, D.A. and Sedat, J.W. (2008) Three-dimensional resolution doubling in wide-field fluorescence microscopy by structured illumination. *Biophys. J.* **94**, 4957–4970.

Haldrup, A., Jensen, P.E., Lunde, C. and Scheller, H.V. (2001) Balance of power: a view of the mechanism of photosynthetic state transitions. *Trends Plant Sci.* **6**, 301–305.

Hayashi, S. and Okada, Y. (2015) Ultrafast superresolution fluorescence imaging with spinning disk confocal microscope optics. *Mol. Biol. Cell*, **26**, 1743–1751.

Heifetz, P.B., Förster, B., Osmond, C.B., Giles, L.J. and Boynton, J.E. (2000) Effects of acetate on facultative autotrophy in *Chlamydomonas reinhardtii* assessed by photosynthetic measurements and stable isotope analyses. *Plant Physiol.* **122**, 1439–1446.

Horton, P., Ruban, A.V. and Walters, R.G. (1996) Regulation of light harvesting in green plants. *Annu. Rev. Plant Physiol. Plant Mol. Biol.* **47**, 655–684.

Iwai, M., Yokono, M. and Nakano, A. (2014) Visualizing structural dynamics of thylakoid membranes. *Sci. Rep.* **4**, 3768.

Iwai, M., Yokono, M., Kurokawa, K., Ichihara, A. and Nakano, A. (2016) Live-cell visualization of excitation energy dynamics in chloroplast thylakoid structures. *Sci. Rep.* **6**, 29940.

Johnson, M.P., Goral, T.K., Duffy, C.D., Brain, A.P., Mullineaux, C.W. and Ruban, A.V. (2011) Photoprotective energy dissipation involves the reorganization of photosystem II light-harvesting complexes in the grana membranes of spinach chloroplasts. *Plant Cell*, **23**, 1468–1479.

Kirchhoff, H., Hall, C., Wood, M., Herbstova, M., Tsabari, O., Nevo, R., Charuvi, D., Shimoni, E. and Reich, Z. (2011) Dynamic control of protein diffusion within the granal thylakoid lumen. *Proc. Natl Acad. Sci. USA*, **108**, 20248–20253.

Kouril, R., Wientjes, E., Bultema, J.B., Croce, R. and Boekema, E.J. (2013) High-light vs. low-light: effect of light acclimation on photosystem II composition and organization in *Arabidopsis thaliana*. *Biochim. Biophys. Acta*, **1827**, 411–419.

Mackinder, L.C.M., Chen, C., Leib, R.D., Patena, W., Blum, S.R., Rodman, M., Ramundo, S., Adams, C.M. and Jonikas, M.C. (2017) A spatial interactome reveals the protein organization of the algal CO_2-concentrating mechanism. *Cell*, **171**, 133–147.e114.

Mizusawa, N., Yamamoto, N. and Miyao, M. (1999) Characterization of damage to the D1 protein of photosystem II under photoinhibitory illumination in non-phosphorylated and phosphorylated thylakoid membranes. *J. Photochem. Photobiol. B*, **48**, 97–103.

Moriyama, T., Toyoshima, M., Saito, M., Wada, H. and Sato, N. (2018) Revisiting the algal "chloroplast lipid droplet": the absence of an entity that Is unlikely to exist. *Plant Physiol.* **176**, 1519–1530.

Mulders, K.J.M., Janssen, J.H., Martens, D.E., Wijffels, R.H. and Lamers, P.P. (2014) Effect of biomass concentration on secondary carotenoids and triacylglycerol (TAG) accumulation in nitrogen-depleted *Chlorella zofingiensis*. *Algal Res.* **6**, 8–16.

Nelson, N. (2011) Photosystems and global effects of oxygenic photosynthesis. *Biochim. Biophys. Acta*, **1807**, 856–863.

Nishiyama, T., Hiwatashi, Y., Sakakibara, I., Kato, M. and Hasebe, M. (2000) Tagged mutagenesis and gene-trap in the moss, *Physcomitrella patens* by shuttle mutagenesis. *DNA Res.* **7**, 9–17.

Niyogi, K.K. (1999) Photoprotection revisited: genetic and molecular approaches. *Annu. Rev. Plant Physiol. Plant Mol. Biol.* **50**, 333–359.

Olsson, T., Thelander, M. and Ronne, H. (2003) A novel type of chloroplast stromal hexokinase is the major glucose-phosphorylating enzyme in the moss *Physcomitrella patens*. *J. Biol. Chem.* **278**, 44439–44447.

Pribil, M., Pesaresi, P., Hertle, A., Barbato, R. and Leister, D. (2010) Role of plastid protein phosphatase TAP38 in LHCII dephosphorylation and thylakoid electron flow. *PLoS Biol.* **8**, e1000288.

Rochaix, J.D. (2014) Regulation and dynamics of the light-harvesting system. *Annu. Rev. Plant Biol.* **65**, 287–309.

Roth, M.S., Cokus, S.J., Gallaher, S.D. *et al.* (2017) Chromosome-level genome assembly and transcriptome of the green alga *Chromochloris zofingiensis* illuminates astaxanthin production. *Proc. Natl Acad. Sci. USA*, **114**, E4296–E4305.

Ruban, A.V. (2016) Nonphotochemical chlorophyll fluorescence quenching: mechanism and effectiveness in protecting plants from photodamage. *Plant Physiol.* **170**, 1903–1916.

Schottkowski, M., Peters, M., Zhan, Y., Rifai, O., Zhang, Y. and Zerges, W. (2012) Biogenic membranes of the chloroplast in *Chlamydomonas reinhardtii*. *Proc. Natl Acad. Sci. USA*, **109**, 19286–19291.

Schumaker, K.S. and Dietrich, M.A. (1997) Programmed changes in form during moss development. *Plant Cell*, **9**, 1099–1107.

Shapiguzov, A., Ingelsson, B., Samol, I., Andres, C., Kessler, F., Rochaix, J.D., Vener, A.V. and Goldschmidt-Clermont, M. (2010) The PPH1 phosphatase is specifically involved in LHCII dephosphorylation and state transitions in *Arabidopsis*. *Proc. Natl Acad. Sci. USA*, **107**, 4782–4787.

Shimoni, E., Rav-Hon, O., Ohad, I., Brumfeld, V. and Reich, Z. (2005) Three-dimensional organization of higher-plant chloroplast thylakoid membranes revealed by electron tomography. *Plant Cell*, **17**, 2580–2586.

Thelander, M., Olsson, T. and Ronne, H. (2005) Effect of the energy supply on filamentous growth and development in *Physcomitrella patens*. *J. Exp. Bot.* **56**, 653–662.

Valkunas, L., Chmeliov, J., Trinkunas, G., Duffy, C.D., van Grondelle, R. and Ruban, A.V. (2011) Excitation migration, quenching, and regulation of photosynthetic light harvesting in photosystem II. *J. Phys. Chem. B*, **115**, 9252–9260.

Wientjes, E., Drop, B., Kouril, R., Boekema, E.J. and Croce, R. (2013) During state 1 to state 2 transition in *Arabidopsis thaliana*, the photosystem II supercomplex gets phosphorylated but does not disassemble. *J. Biol. Chem.* **288**, 32821–32826.

Wobbe, L., Bassi, R. and Kruse, O. (2016) Multi-level light capture control in plants and green algae. *Trends Plant Sci.* **21**, 55–68.

Wood, W.H.J., MacGregor-Chatwin, C., Barnett, S.F.H., Mayneord, G.E., Huang, X., Hobbs, J.K., Hunter, C.N. and Johnson, M.P. (2018) Dynamic thylakoid stacking regulates the balance between linear and cyclic photosynthetic electron transfer. *Nat. Plants*, **4**, 116–127.

Zhang, Z., Sun, D., Mao, X., Liu, J. and Chen, F. (2016) The crosstalk between astaxanthin, fatty acids and reactive oxygen species in heterotrophic *Chlorella zofingiensis*. *Algal Res.* **19**, 178–183.

